Desalination and Water Treatment
www.deswater.com
doi: 10.1080/19443994.2014.922444

55 (2015) 1040–1047
July

Taylor & Francis
Taylor & Francis Group

Removal of reactive dye from aqueous solution using thermally treated red mud

Carolina Petrisin Costa de Jesus[a], Maria Lúcia Pereira Antunes[a], Fabiano Tomazini da Conceição[b,*], Guillermo Rafael Beltran Navarro[b], Rodrigo Braga Moruzzi[b]

[a]*Departamento de Engenharia Ambiental, UNESP—Univer. Estadual Paulista, Avenida Três de Março, 511, 18087-180 Sorocaba, SP, Brasil, emails: ftomazini@hotmail.com (C.P.C de Jesus), malu@sorocaba.unesp.br (M.L.P Antunes)*
[b]*Instituto de Geociências e Ciências Exatas, UNESP—Univer. Estadual Paulista, Avenida 24-A, nº 1515, CEP 13506-900, Bela Vista, Rio Claro, SP, Brasil, emails: ftomazini@rc.unesp.br (F.T. da Conceição), grbnavarro@yahoo.com (G.R.B Navarro), rmoruzzi@rc.unesp.br (R.B. Moruzzi)*

Received 16 December 2013; Accepted 26 April 2014

ABSTRACT

The removal of color from wastewater is a major problem for textile industries. The best option to remove color is to combine conventional treatments with additional processes, such as adsorption. Industrial waste has been studied for use as adsorbents, specifically red mud (RM), which is an insoluble residue that is generated in large quantities during the processing of bauxite. In this study, a typical reactive dye, reactive blue 19 dye (RB 19), used in the textile industry was selected, and its ability to adsorb RM that was thermally treated at 500˚C (RM 500˚C) was evaluated. The adsorption of RB 19 was highest when the pH values were lower than the pH_{PCZ} (7.0). The experimental adsorption capacity data were analyzed using the Langmuir and Freundlich models. The Langmuir model was more appropriate for describing this phenomenon in acidic conditions, with a maximum adsorption capacity of 178.4 mg g^{-1} (R^2 of 0.84). Kinetics studies indicate that a pseudo-second-order reaction mechanism is responsible for the adsorption of RB 19, indicating that adsorption occurs through electrostatic interactions. Thus, these results indicate that the RM 500˚C has potential applications for treating effluents from textile industries.

Keywords: Bauxite refining residue; Reactive dye adsorption; Kinetics studies; Isotherms models

1. Introduction

The textile industry is greatly important to the economies of emerging countries. Brazil is the largest textile center in South America, ranking fifth among the largest producers of textiles and clothing in the world [1]. Water consumption and the generation of large volumes of industrial effluents that have high concentrations of dyes and chemicals are associated with the high-economic performance of the industry. The direct discharge of dye into water bodies can cause serious environmental problems by reducing light penetration into the water column and photosynthesis [2].

The best option for removing color from wastewater is to combine conventional treatments with additional processes such as chemical oxidation [3–5],

*Corresponding author.

membrane filtration [6], adsorption [7], and coagulation [8]. The adsorption technique presents the best results for industrial applications [9]. Adsorbents such as activated carbon [10,11], clay [12,13], chitosan and chitin [14,15], and cellulosic materials [16] are commonly used to remove dyes from industrial wastewater.

Good results have been obtained with different alternative and inexpensive materials [17–19], especially red mud (RM), which is an insoluble residue created in large quantities during the refining of bauxite ore. Brazil produces a third of the world's bauxite, surpassed only by Australia and China. Bauxite refining residue (RM) is derived from the Bayer process during the digestion of crushed bauxite in a concentrated caustic solution (NaOH) at elevated temperatures and pressures. In Brazil, 7,000,000–10,500,000 tons of this insoluble residue is generated per year during the refining of bauxite ore [20]. The residues occupy vast areas. Apart from the visual impact, they can leak and consequently contaminate the soil, surface water, and groundwater [21–23].

In the present study, a typical reactive dye from the textile industry was selected, and its adsorption onto Brazilian thermally treated RM was investigated. For this study, the pH, electrical conductivity, isoelectric point, mineralogy, and surface area of natural RM and RM that was thermally treated at 500˚C (RM 500˚C) were characterized. The influence of the initial pH on the adsorption tests using RM that was thermally treated at 500˚C was evaluated. Pseudo-first-order and pseudo-second-order kinetics models and adsorption isotherms were studied to understand the dye adsorption characteristics of the RM 500˚C. The kinetic models were based on Langmuir and Freundlich models.

2. Materials and methods

2.1. RM activation and characterization

Brazilian RM samples were provided by the aluminum plant in Alumínio City, São Paulo State, Brazil. Initially, all of the samples of RM were dried overnight at 80˚C. According to Antunes et al. [24], Brazilian RM has been classified as mesoporous at all temperatures, except between 400 and 500˚C, where a better gain of specific surface area was observed. Thus, the heating treatment used for the RM was conducted at 500˚C in a furnace for 3 h (RM 500˚C).

The pH and the electrical conductivity values for RM and RM 500˚C were determined using a YSI 556 meter calibrated with standard solutions: pH 4.00 (4.00 ± 0.01 at 25˚C ± 0.2˚C) and 7.00 (7.00 ± 0.01 at 25˚C ± 0.2˚C) and a solution of KCl (1.0 mmol L^{-1}) of known electrical conductivity: 147 μS cm^{-1} at 25˚C.

The pH of the isoelectric point (pH_{PCZ}) was also determined from RM and RM 500˚C. NaCl solutions (0.1 N) with pH values ranging from 1 to 11 were prepared. RM and RM 500˚C (0.10 g) were added to the solutions. This system was continuously stirred at 250 rpm at room temperature for 48 h. After this period, the final pH of the solutions was measured. The pH_{PCZ} is defined as the point on the pH_{final} versus $pH_{initial}$ curve that crosses the line $pH_{final} = pH_{initial}$ [25].

The mineral composition was determined by X-Ray diffraction (XRD) using a Philips X-Pert wide-angle X-ray diffractometer operating at 40 kV and 40 mA with CuKα radiation. The morphologies of the RM and RM 500˚C samples were observed using a scanning electron microscope equipped with an energy dispersive X-ray spectrometer unit (SEM-EDS). The specific surface areas of all samples were determined by BET/N_2 adsorption methods using a Micromeritics ASAP 2010 instrument.

2.2. Adsorption studies

The adsorption experiments were carried out with RM 500˚C as the adsorbent and the Reactive Blue 19 (RB 19) dye as the adsorbate. The characteristics of the dye are shown in Table 1. Aqueous solutions of this dye show maximum adsorbance at 590 nm in the visible region. The pH range does not affect the adsorbance of the dye. The time required to reach adsorption equilibrium of RB 19 was 3 h.

Isothermal studies were carried out by mixing 0.200 g (±0.01 g) of RM 500˚C with 50 mL of a RB 19 solution with the following concentrations: 100, 500, 1,000, 2,000, 3,000, and 5,000 mg L^{-1}. The samples with initial concentrations higher than 500 mg L^{-1} of dye, were diluted 1:200 in distilled water. The system was continuously stirred at 250 rpm for 3 h and maintained at a temperature of 30˚C. Next, the solution was centrifuged for 3 minutes at 3500 rpm, and an aliquot was collected from the supernatant to determine the residual RB 19 concentration. The influence of the initial pH on the experiments was studied using solutions with pH values of 2.0, 4.0, 7.0, and 10.0.

The adsorption kinetics study was carried out by monitoring the concentration of RB 19 over time, which consisted of adding 0.200 g (±0.01 g) of RM 500˚C at different concentrations (500, 1000, and 1500 mg L^{-1}) to 50 mL of a RB 19 solution at pH 4. After different time intervals, an aliquot of the sample was centrifuged to determine the residual concentration of RB 19.

Table 1
Main characteristics of the reactive blue 19 dye (RB19)

Molecular structure	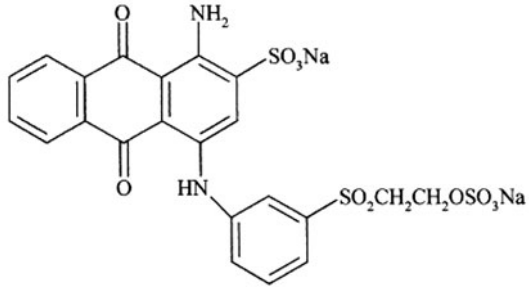
Generic name	C.I. Reactive blue 19
Molecular formula	$C_{22}H_{16}N_2O_{11}S_3Na_2$
Molar mass	626.54 g mol^{-1}
Class	Reactive
$\lambda_{máx}$ (nm)	590

The RB 19 residual concentrations were determined using a Hach DR-2800 spectrophotometer with peak readings centered at a wavelength of 590 nm. Deionized water was used as a blank sample. The amount of RB 19 adsorbed onto the RM, q_e (mg g^{-1}), was calculated using the mass-balance relationship shown in Eq. (1). The percent adsorption (%A) of RB 19 was calculated using Eq. (2).

$$q_e = \frac{(C_0 - C_e) \times V}{W} \quad (1)$$

$$\%A = \frac{(C_0 - C_e)}{C_0} \times 100 \quad (2)$$

where C_0 and C_e = initial and equilibrium concentrations of dye, respectively (mg L^{-1}); V = volume of solution (L); W = weight of adsorbent sample (g).

3. Results and discussion

3.1. Characterization of Brazilian RM

The procedure for determining the chemical composition of RM and RM 500 °C has been described by Antunes et al. [24]. The results indicate that the main constituents of these materials are Fe_2O_3, Al_2O_3, and SiO_2 (Table 2). The grain size analysis indicated that the RM and RM 500 °C have ca. 7% of fine sand (>0.05 mm), 60% of silt (from 0.002 to 0.02 mm), and 33% of clay (<0.002 mm) [24]. The characteristics of RM and RM 500 °C are shown in Table 3. The pH values of RM and RM 500 °C are 10.3 and 10.9, respectively, which confirms that the material is highly alkaline even after heat treatment due to the addition of NaOH in the Bayer process.

Table 2
Chemical composition (%) of RM and RM 500 °C

Oxide	RM	RM 500 °C
SiO_2	19.2	20.7
TiO_2	3.0	3.2
Al_2O_3	22.8	24.3
Fe_2O_3	27.4	28.9
MnO	0.2	0.2
MgO	0.4	0.4
CaO	2.2	2.3
Na_2O	7.9	8.0
K_2O	0.8	0.8
P_2O_5	0.4	0.4
LOI	15.5	10.4
Total	99.8	99.6

The activation of RM 500 °C reduces the electrical conductivity of this material from 3,700 to 1,600 μS cm^{-1}. The pH_{PCZ} (7.0) appears to be unaffected by the heat treatment. Furthermore, thermal activation at 500 °C increases the specific surface area of the material from 18.7 to 38.0 m^2 g^{-1}, with pore sizes ranging from 1 to 4 nm, corresponding to the dimensions of mesopores and micropores. The morphologies of the RM and RM 500 °C particles were observed using SEM-EDS, as illustrated in Fig. 1. RM and RM 500 °C samples are composed of particles with different sizes and forms. The heat treatment does not appear to change the morphology of the particles.

Fig. 2 shows the XRD patterns of RM and RM 500 °C. The mineralogical composition of RM shows

Table 3
Characterization of RM and RM 500°C

Parameter	RM	RM 500°C
pH	10.3	10.9
Electrical conductivity ($\mu S\,cm^{-1}$)	3,700	1,600
Specific surface area ($m^2\,g^{-1}$)	18.7	38.0
pH_{PCZ}	7.0	7.0
Mineralogy	hematite, goethite, quartz, gibbsite, calcite, sodalite, kaolinite, and rutile	hematite, quartz, alumina, calcite, sodalite, kaolinite, and rutile

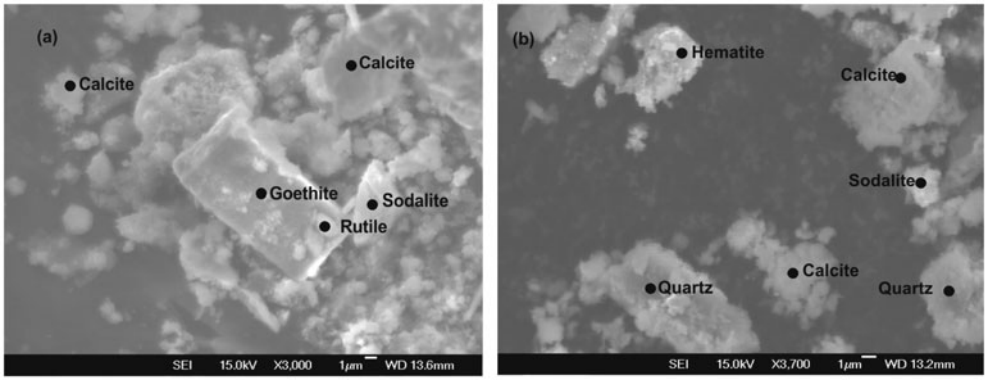

Fig. 1. SEM-EDS of RM (a) and RM 500°C (b).

that hematite (Fe_2O_3), goethite (FeO(OH)), quartz (SiO_2), gibbsite ($Al(OH)_3$), calcite ($CaCO_3$), sodalite ($Na_8Al_6Si_6O_{24}Cl_2$), kaolinite ($Al_2Si_2O_5(OH)_4$), and rutile (TiO_2) were present in the samples. The peaks corresponding to gibbsite and goethite are no longer observed in the XRD patterns of RM 500°C, while the intensity and sharpness of the hematite bands increase (See the marked regions on Fig. 2). This behavior is particularly obvious for the hematite band at approximately 33° 2θ CuKα. According to Antunes et al. [24], the decomposition of goethite to hematite occurred at 234°C ($FeO(OH) \rightarrow Fe_2O_3$) and the gibbsite decomposed to boehmite and then to alumina at 272°C ($Al(OH)_3 \rightarrow Al(OH)_{(S)} + H_2O \rightarrow Al_2O_3 + H_2O$). This explains the increase of specific surface area in RM 500°C because the transition aluminas have a higher specific surface area than the original hydroxides [26].

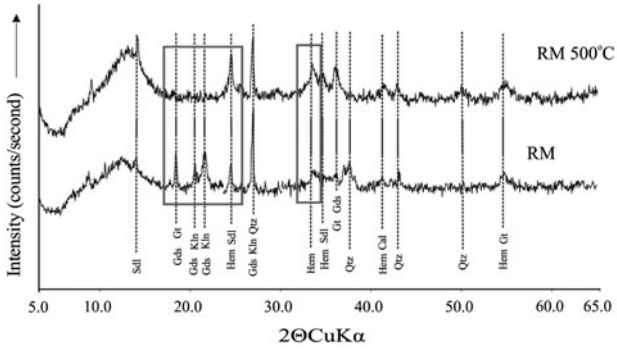

Fig. 2. XRD patterns of RM and RM 500°C. Sodalite = Sdl, Gibbsite = Gds, Goethite = Gt, Kaolinite = Kln, Hematite = Hem, Quartz = Qtz, and Calcite = Cal. The marked regions emphasize the disappearance of peaks of the aluminum and iron hydroxides.

3.2. Influence of pH on adsorption experiments

Fig. 3 shows the removal of RB 19 by RM 500°C at different pH conditions (pH values of 2, 4, 7, and 10). The removal efficiency of RB 19 decreases as the initial concentration of RB 19 increases for all pH values. This result is due to the limited number of surface sites available for adsorption, which will be occupied by the RB 19 molecules during the adsorption process [27]. When the concentration of RB 19 in solution increases, the competition for vacant sites increases (limited sites available). After reaching saturation, no more dye can be adsorbed.

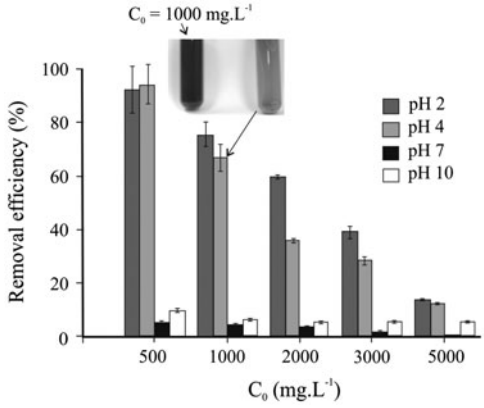

Fig. 3. The effect of initial pH on the adsorption of RB 19 by RM 500˚C under different pH conditions.

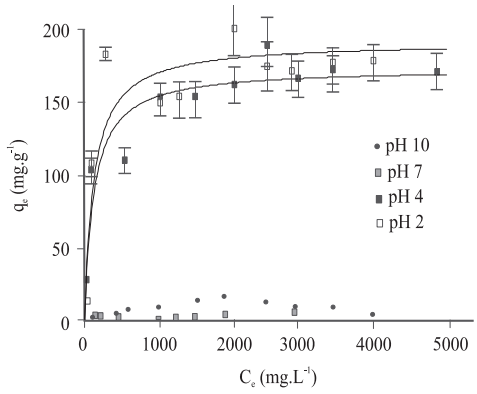

Fig. 4. Adsorption isotherms of RB19 by RM 500˚C using the Langmuir adsorption model for pH 2 and 4.

For all concentrations tested, the percent removal of RB 19 was between 5 and 10% at alkaline pH (10.0), indicating a weak adsorption process. For all concentrations, the adsorption capacity was significantly increased under acidic conditions, (pH values of 2 and 4). For solutions with an initial concentration of RB 19 below 500 mg L^{-1}, the color removal capacity exceeded 90% under acidic conditions. However, the percent adsorption for all concentrations was very low in solutions with a pH of approximately 7 near the pH_{PCZ}. This result confirms that when the surface charge of RM 500˚C is neutral, the RM has the lowest adsorption capacity.

3.3. Adsorption isotherms

Fig. 4 shows the isotherms for the adsorption of RB 19 dye onto RM 500˚C. The isotherms describe the equilibrium relationship between the concentration of an adsorbate on the solid phase and its concentration in the liquid phase at constant temperature and pressure. Analysis of these isotherms was performed by adjusting Langmuir and Freundlich adsorption models.

The Langmuir model (Eq. (3)) assumes that maximum adsorption corresponds to a saturated monolayer of adsorbate molecules on the surface of the adsorbent with a constant energy. The constants K_L and q_m can be obtained by rearranging Eq. (3), resulting in Eq. (4).

$$q_e = \frac{(q_m \times K_L \times C_e)}{(1 + K_L \times C_e)} \tag{3}$$

$$\frac{C_e}{q_e} = \frac{1}{q_m \times K_L} + \left(\frac{1}{q_m}\right) \times C_e \tag{4}$$

where K_L = the Langmuir constant related to the energy of adsorption (mg^{-1}); q_m = maximum amount of adsorption corresponding to complete monolayer coverage on the surface (mg g^{-1}).

The Freundlich model is an empirical isotherm that can be used for non-ideal sorption involving heterogeneous surface energy systems. Eq. (5) describes this model, and the linear form is written in Eq. (6).

$$q_e = K_F \times C_e^{\frac{1}{n}} \tag{5}$$

$$\log q_e = \log K_F + \left(\frac{1}{n}\right) \times \log C_e \tag{6}$$

where K_F = Freundlich constant; n = constant ($1/n$ is the adsorption intensity).

The abovementioned isotherms were used to adjust the experimental data, and the results are shown in Table 4. The Langmuir model represents RB 19 adsorption onto RM 500˚C when the system is acidic. However, for alkaline pH conditions, the use of Freundlich model is more appropriated. These results show that the adsorption of RB 19 under acidic conditions resulted into a saturated monolayer of dye on the RM adsorbent (Langmuir model). At pH 4.0, each gram of RM 500˚C shows a maximum adsorption capacity of 168.7 mg of RB 19, whereas at pH 2.0, the same amount of adsorbent material is capable of adsorbing 178.4 mg of this dye. Under acidic adsorption conditions, the average maximum adsorption capacity of RM that was thermally treated at 500˚C is 173 ± 7 mg g^{-1}.

Table 4
Adsorption parameters using Langmuir and Freundlich models for RM 500℃

	pH 2.0	pH 4.0	pH 7.0	pH 10.0
Langmuir parameters				
q_m (mg g^{-1})	178.4	168.7	−1.95	248.65
K_L	0.005	0.009	1.0	0.0001
R^2	0.84	0.96	0.65	0.22
Freundlich parameters				
n	2.75	3.04	2.72	1.02
K_F (mg g^{-1}) (L mg^{-1})$^{1/n}$	11.8	13.3	0.85	0.26
R^2	0.51	0.74	0.46	0.95

3.4. Adsorption kinetic studies

In this study, adsorption kinetic was obtained for the acidic conditions using different initial concentrations (Fig. 5). It is important to know the rate of adsorption from kinetics models to design wastewater treatment systems for industrial plants. The Lagergren pseudo-first-order (Eq. (7)) and pseudo-second-order (Eq. (8)) models were used to understand the dynamics of the adsorption kinetics of RB 19 by RM 500℃.

$$\frac{dq_t}{dt} = K_1 \times (q_e - q_t) \tag{7}$$

$$\frac{dq_t}{dt} = K_2 \times (q_e - q_t)^2 \tag{8}$$

where q_e and q_t = amount of RB 19 adsorbed (mg g^{-1}) at equilibrium and at any time t (min), respectively; K_1 and K_2 = the equilibrium rate constants of pseudo-first-order (min^{-1}) and pseudo-second-order adsorption (g mg^{-1} min^{-1}), respectively.

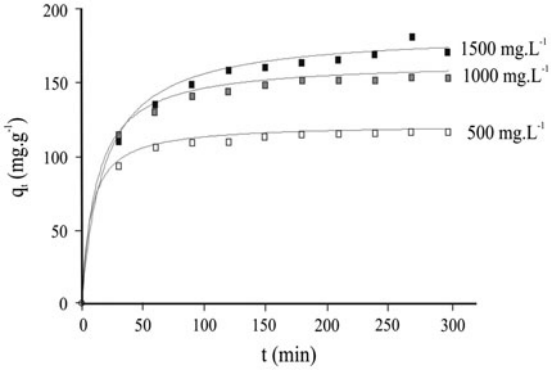

Fig. 5. Kinetic curves for adsorption of RB19 by RM 500℃ at pH 4, with lines indicating the pseudo-second-order model.

It is possible to write Eqs. (9) and (10) by integrating Eqs. (7) and (8) with the boundary conditions $t = 0$ to t and $q_t = 0$ to q_t and rearranging them to obtain a linear form.

$$\log\,(q_e - q_t) = \log q_e - \left(\frac{K_1}{2.303}\right) \cdot t \tag{9}$$

$$\frac{t}{q_t} = \left(\frac{1}{K_2 \cdot q_e^2}\right) + \left(\frac{1}{q_e}\right) \cdot t \tag{10}$$

The results of the adsorption kinetics of pseudo-first-order and pseudo-second-order models for RB 19 by RM 500℃ are shown in Table 5. The adjustment coefficient for the pseudo-second-order model is a better fit to the experimental data with a value of 0.99. Additionally, the calculated values of q_e are closer to the experimental values of q_e. This result indicates that the adsorption of RB 19 by RM 500℃ obeys the pseudo-second-order kinetic model. The pseudo-second-order kinetic model is based on the assumption that the rate-limiting step may involve valence forces such as electron sharing or exchange between sorbent and sorbate [28]. The pH_{PCZ} measure confirms such an adsorption mechanism.

In addition, the kinetic data (q_t and t) can be plotted in Elovich Eq. (11), which assumes that the solid surface active sites are heterogeneous in nature [29,30]. In this equation, α and β are related to the rate of initial adsorption (chemisorption) and surface coverage (desorption constant), respectively. The intraparticle diffusion kinetic model (Eq. 12) considers that the adsorbate species are mostly transported from the bulk of the solution into the solid phase through intraparticle diffusion/transport [29,30]. The values of the coefficients of Elovich and intraparticle diffusion equations are listed in Table 6.

$$q_t = \frac{1}{\beta}\,\ln\,(\alpha\beta) + \frac{1}{\beta}\,\ln t \tag{11}$$

Table 5
Pseudo-first and pseudo-second-order adsorption rate constants and the calculated and experimental q_e values for adsorption of RB19 by RM 500˚C at pH 4

		First-order kinetic model			Second-order kinetic model		
C_0 (mg/L)	q_e (exe) (mg g^{-1})	K_1 (min^{-1})	q_e (cal) (mg g^{-1})	R^2	K_2 (g mg^{-1} min^{-1})	q_e (cal) (mg g^{-1})	R^2
500	117	0.014	50	0.88	0.0011	119	0.99
1,000	155	0.015	84	0.93	0.0005	161	0.99
1,500	172	0.015	124	0.98	0.0003	181	0.99

Table 6
Elovich and intraparticle diffusions parameters for adsorption of RB19 by RM 500˚C at pH 4

	Elovich parameters			Intraparticle diffusion parameters		
C_0 (mg/L)	α (mg g^{-1} min^{-1})	β (mg g^{-1})	R^2	k_i (mg g^{-1} min$^{-0.5}$)	C (mg g^{-1})	R^2
500	60.49	0.03	0.95	8.89	42.94	0.83
1,000	515.03	0.06	0.94	3.09	105.97	0.84
1,500	13,807.19	0.11	0.92	1.61	90.79	0.81

$$q_t = k_i t^{0.5} + C \quad (12)$$

where α = initial adsorption rate constant (mg g^{-1} min^{-1}); β = desorption constant (mg g^{-1}); k_i = intraparticle diffusion rate constant (mg g^{-1} min$^{-0.5}$); C = intercept (mg g^{-1}).

The correlation coefficients (R^2) indicate a linear characteristic, with values ranging from 0.92 to 0.95 and 0.81 to 0.84 for Elovich and intraparticle diffusion kinetic models, respectively. With the increase in initial concentration (C_0), the constants α and β increased, suggesting that both the rate of chemisorption and the available adsorption surface would increase. When the q_t versus $t^{0.5}$ plots pass through the origin, the intraparticle diffusion is the rate-limiting step. With the intercept values present in Table 6, it is possible to conclude that surface adsorption and intraparticle diffusion were concurrently operating during the adsorption of RB19 by RM 500˚C at pH 4.

4. Conclusions

The chemical and mineralogical analysis showed that heat treatment of RM at 500˚C transforms the hydroxides in oxides, thereby increasing the specific surface area of this material. The pH_{PCZ} was equal for samples of RM and RM 500˚C. The adsorption was significantly dependent on the pH of the solution. Acidic conditions proved to be optimal for adsorption. The highest percent removal of RB 19 by RM 500˚C occurred at pH values lower than the pH_{PCZ}, which were acidic solutions. The Langmuir model was more appropriate for describing the removal of RB 19 in acidic solutions. The average maximum adsorption capacity of thermally treated RM is 178.4 mg g^{-1}. The pseudo-second-order kinetic model was a better fit for the experimental data, which indicates that electrostatic interaction is the main adsorption mechanism. Thus, this study indicates that the RM 500˚C has a high capacity for removing RB 19, which suggests that this bauxite refining residue has potential applications in the treatment of effluents from textile industries.

Acknowledgment

This investigation was supported by the Fundação de Amparo à Pesquisa do Estado de São Paulo (FAPESP—Process No. 2009/02374-0) and the Conselho Nacional de Desenvolvimento Científico e Tecnológico (CNPq—Process No. 480555/2009-5). We would like to especially acknowledge the Companhia Brasileira de Alumínio (CBA) for making red mud samples available. Three anonymous referees are thanked for comments that helped to improve the manuscript.

References

[1] ABIT – Associação Brasileira da Indústria Têxtil e de Confecção, 2011. Available from: www.abit.org.br/site/navegacao.asp?id_menu=1&id_sub=4&idioma=PT.

[2] S.B. Wang, Y. Boyjoo, A. Choueib, Z.H. Zhu, Removal of dyes form aqueous solution using fly ash and red mud, Water Res. 39 (2005) 129–138.
[3] N. Mohan, N. Balasubramanian, V. Subramanian, Electrochemical treatment of simulated textile effluent, Chem. Eng. Technol. 24 (2001) 749–753.
[4] S.K. Ling, S. Wang, Y. Peng, Oxidative degradation of dyes in water using Co^{2+}/H_2O_2 and Co^{2+}/peroxymonosulfate, J. Hazard. Mater. 178 (2010) 385–389.
[5] J.L. Figueiredo, J.P.S. Sousa, C.A. Orge, M.F.R. Pereira, J.J.M. Orfão, Adsorption of dyes on carbon xerogels and templated carbons: influence of surface chemistry, Adsorption 17 (2011) 431–441.
[6] J. Sojka-Ledakowicz, R. Zylla, Z. Mrozinska, K. Pazdzior, A. Klepacz-Smolka, S. Ledakowicz, Application of membrane processes in clothing of water cycle in textile dyehouse, Desalination 250 (2010) 634–638.
[7] V.K. Gupta, Suhas, Application of low cost adsorbents for dye removal – A review, J. Environ. Manag. 90 (2009) 2313–2342.
[8] R.J. Stephenson, S.J.B. Duff, Coagulation and precipitation of mechanical pulping effluent 0.1 Removal of carbon, colour and turbidity, Water. Res. 30 (1996) 781–792.
[9] M. Sharma, R.K. Vyas, K. Singh, A review on reactive adsorption for potential environmental applications, Adsorption 19 (2013) 161–188.
[10] M. Walker, L.R. Weatherley, Adsorption of dyes from aqueous solution: The effect of adsorbent pore size distribution and dye aggregation, Chem. Eng. J. 83 (2001) 210–206.
[11] S. Papic, N. Koprivanac, A.L. Bozic, A. Metes, Removal of some reactive dyes from synthetic waste water by combined Al(III) coagulation/carbon adsorption process, Dyes Pigm. 62 (2004) 291–298.
[12] M. Alkan, S. Celikcapa, O. Demirbas, M. Dogan, Removal of reactive blue 221 and acid blue 62 anionic dyes from aqueous solutions by sepiolite, Dyes Pigm 65 (2005) 251–259.
[13] F.G.E. Nogueira, J.H. Lopes, A.C. Silva, M. Gonçalves, A.S. Anastácio, K. Sapag, L.C.A. Oliveira, Reactive adsorption of metlhylene blue on montmorillonite via na ESI-MS study, Appl. Clay Sci. 43 (2009) 190–195.
[14] R.S. Juang, R.L. Tseng, F.C. Wu, S.H. Lee, Adsorption behavior of reactive dyes from aqueous solution on chitosan, J. Chem. Technol. Biotechnol. 70 (1997) 391–399.
[15] P. Longhinotti, F. Pozza, L. Furlan, M.N.M. Sanches, M. Klug, M. Laranjeira, V.T. Fávere, Adsorption of anionic dyes on the biopolymer chitin, J. Braz. Chem. Soc. 9 (1988) 435–440.
[16] A. Bousher, X. Shen, R.G.J Edyvean, Removal of coloured organic matter by adsorption onto low-cost waste materials, Water Res 31 (1997) 2084–2092.
[17] K. Gupta, Suhas, V.K. Saini, Removal of rhodamine B, fast green and methylene blue from wastewater using red mud, an aluminum industry waste, Ind. Eng. Chem. Res. 43 (2004) 1740–1747.
[18] S. Wang, H.M. Ang, M.O. Tadé, Novel applications of red mud as coagulant, adsorbent and catalyst for environmental benign process, Chemosphere 72 (2008) 1621–1635.
[19] V.K. Gupta, P.J.M. Carrot, M.M.L. Ribeiro Carrot, Suhas, Low-cost adsorbents: Growing approach to waste water treatment – A review, Crit. Rev. Environ. Sci. Technol. 39 (2009) 783–842.
[20] J.M.R. Mercury, A.A. Cabral, A.E.M. Paiva, R.S. Angelica, R.F. Neves, T. Scheller, Thermal behavior and evolution of the minerals phases of Brazilian red mud, J. Therm. Anal. Calorim. 104 (2011) 634–643.
[21] M. Enserink, After red mud flood, scientists try to halt wave of fear and rumors, Science 330 (2010) 432–433.
[22] A. Gelencser, N. Kovats, B. Turoczi, A. Rostasi, A. Hoffer, K. Imre, I. Nyirõ-kósa, D. Csakberényi-Malasics, A. Czitovszky, A. Nagy, S. Nagy, A. Ács, A. Kovács, Á. Ferincz, Z. Hartyáni, M. Pósfai, The red mud accident in Ajka (Hungary): Characterization and potential health effects of fugitive dust, Environ. Sci. Technol. 45 (2011) 1608–1615.
[23] W.A. Mayes, A.P. Jarvis, I.T. Burke, M. Walton, V. Feigl, O. Klebercz, K. Gruiz, Dispersal and attenuation of trace contaminants downstream of the Ajka bauxite residue (red mud) depository failure, Hungary. Environ. Sci. Technol. 45 (2011) 5147–5155.
[24] M.L.P. Antunes, S.J. Couperthwaite, F.T. Conceicão, C.P.C. Jesus, P.K. Kiyohara, A.C.V. Coelho, R.L Frost, Red mud from Brazil: Thermal behavior and physical properties, Ind. Eng. Chem. Res. 51 (2012) 775–779.
[25] J.J.M. Orfão, A.I.M. Silva, J.C.V. Pereira, S.A. Barata, I.M. Fonseca, P.C.C. Faria, M.F.R. Pereira, Adsorption of reactive dye on chemically modified activated carbons – Influence of pH, J. Colloid Interface Sci. 296 (2006) 480–489.
[26] K. Wefers, C. Misra, Oxides and Hydroxides of Aluminium. Technical Paper no. 19, ALCOA Reserch Laboratories Center, Pittsburg, PA, 1987, p. 3, 15069.
[27] T.E.M. Carvalho, D.A. Fungaro, J.C. Izidoro, Adsorção do corante reativo laranja 16 de soluções aquosas por zeólita sintética [Adsorption of reactive orange 16 from aqueous solutions by synthesized zeolite], Química Nova 33 (2010) 358–363.
[28] Y.S. Ho, G. McKay, Kinetic models for the sorption of dye from aqueous solution by wood, Process Saf. Environ. Prot. 76 (1998) 183–191.
[29] Y. Onal, Kinetics of adsorption of dyes from aqueous solution using activated carbon prepared from waste apricot, J. Hazard. Mater. B137 (2006) 1719–1728.
[30] S. Chowdhury, R. Mishra, P. Saha, P. Kushwaha, Adsorption thermodynamics, kinetics and isoteric heat of adsorption of malachite green onto chemically modified rice husk, Desalination 265 (2011) 159–168.